



OPEN ACCESS

EDITED BY

Rita Graceffa,
European X-Ray Free Electron Laser,
Germany

REVIEWED BY

Zhong Yin,
European X-Ray Free Electron Laser,
Germany
Pietro Parisse,
National Research Council (CNR), Italy

*CORRESPONDENCE

Jonathan C. T. Barnard,
j.barnard16@imperial.ac.uk

SPECIALTY SECTION

This article was submitted
to Structural Biology,
a section of the journal
Frontiers in Molecular Biosciences

RECEIVED 14 September 2022

ACCEPTED 01 November 2022

PUBLISHED 14 November 2022

CITATION

Barnard JCT, Lee JP, Alexander O,
Jarosch S, Garratt D, Picciuto R,
Kowalczyk K, Ferchaud C, Gregory A,
Matthews M and Marangos JP (2022),
Delivery of stable ultra-thin liquid sheets
in vacuum for
biochemical spectroscopy.
Front. Mol. Biosci. 9:1044610.
doi: 10.3389/fmolb.2022.1044610

COPYRIGHT

© 2022 Barnard, Lee, Alexander,
Jarosch, Garratt, Picciuto, Kowalczyk,
Ferchaud, Gregory, Matthews and
Marangos. This is an open-access article
distributed under the terms of the
[Creative Commons Attribution License
\(CC BY\)](#). The use, distribution or
reproduction in other forums is
permitted, provided the original
author(s) and the copyright owner(s) are
credited and that the original
publication in this journal is cited, in
accordance with accepted academic
practice. No use, distribution or
reproduction is permitted which does
not comply with these terms.

Delivery of stable ultra-thin liquid sheets in vacuum for biochemical spectroscopy

Jonathan C. T. Barnard*, Jacob P. Lee, Oliver Alexander, Sebastian Jarosch, Douglas Garratt, Rose Picciuto, Katarzyna Kowalczyk, Clement Ferchaud, Andrew Gregory, Mary Matthews and Jon P. Marangos

Extreme Light Consortium, Blackett Laboratory, Imperial College London, Department of Physics, London, United Kingdom

The development of ultra-thin flat liquid sheets capable of running in vacuum has provided an exciting new target for X-ray absorption spectroscopy in the liquid and solution phases. Several methods have become available for delivering in-vacuum sheet jets using different nozzle designs. We compare the sheets produced by two different types of nozzle; a commercially available borosilicate glass chip using microfluidic channels to deliver colliding jets, and an in-house fabricated fan spray nozzle which compresses the liquid on an axis out of a slit to achieve collision conditions. We find in our tests that both nozzles are suitable for use in X-ray absorption spectroscopy with the fan spray nozzle producing thicker but more stable jets than the commercial nozzle. We also provide practical details of how to run these nozzles in vacuum.

KEYWORDS

XUV spectroscopy, spectroscopy in liquids, microfluidics, liquids in vacuum, interferometry, liquid flatjet

1 Introduction

With the proliferation of lab-scale high harmonic generation (HHG) sources capable of producing isolated sub-femtosecond X-ray pulses (Goulielmakis et al., 2008) and the recent advent of X-ray free electron laser (XFEL) technology capable of producing the same (Joseph et al., 2020), ultrafast X-ray spectroscopy is able to provide unparalleled access to the electronic states and dynamics of a system during photon initiated reactions with sub-femtosecond resolution. Recent work has elucidated ultrafast exciton localisation in organic semiconductors (and other solid examples) (Garratt et al., 2022), and many experiments have been performed in the gas phase following ionisation or excitation and tracked the subsequent electronic and structural changes (Attar et al., 2015; Schnorr et al., 2019).

There are important motivations for using liquid targets for X-ray experiments, given the access to element-specific and ultrafast dynamics these experiments can provide. The majority of important and under-studied chemical and biological processes occur in the solution phase, so in order to provide results that are more representative of real systems, a

solution-phase target is desirable. The presence of neighbouring molecules, either solvent or other solutes, is known to have a large effect on electron dynamics compared to isolated systems (Jordan et al., 2020). As liquid targets refresh themselves between shots they are self-healing, so the concerns about damage or photobleaching that exist in solid targets are avoided with flowing liquid targets, allowing for experiments with stronger fields.

Access to photo-induced dynamics in the liquid or solution phase at few-femtosecond timescales *via* soft X-ray absorption spectroscopy is still in its infancy, with the first reported study in 2020 (Smith et al., 1988). This is partly due to the difficulty of delivering thin liquid targets in vacuum, where extreme ultraviolet (XUV) and soft X-ray beams can be used. If using an HHG source X-ray flux becomes a key concern, so the absorption due to silicon nitrate windows in flow cells or the relatively thick conventional cylindrical jets can render signal transmission close to zero, and furthermore the curvature of the surface in the cylindrical jets induces a focusing that can lead to beam distortion. Spherical droplets suffer the same drawback, significant focusing that ionises the droplet, and scattering of the detected light. Therefore, for soft X-ray absorption spectroscopy with HHG sources windowless, stable and thin flat sheets (or flatjets) are preferable.

Several liquid sheet jet designs capable of producing sheets on the order of 1 μm have been published (Ekimova et al., 2015; Galinis et al., 2017; Ha et al., 2018; Koralek et al., 2018). This paper discusses the working principles and design of two types of microfluidic jets, comparing the dimensions and stability of the sheets produced, in particular focusing on vacuum performance essential for XUV spectroscopy. These types are a gas dynamic virtual nozzle (GDVN) first presented by Koralek et al. (2018), and a fan spray type nozzle first presented by Galinis et al. (2017). In both jets the liquid sheet forms on the exit to the nozzles and this work therefore complements a recent study by Chang et al. (2022), where the temperature dependence of sheets produced by both the externally colliding jets and the GDVN was examined. We also present details of our vacuum system and some pointers to address common pitfalls of using these targets in vacuum.

2 Materials and methods

The basic principle for creating a liquid flatjet relies on appropriate momentum transfer to cause thinning and flattening in one direction. Two streams of liquid collide at a controlled angle. The opposing horizontal momentum components cancel out, which leads to the sheet spreading out radially in the plane of the collision due to the incompressibility of the liquid. If the angle between the flows of liquid that collide is not 180° (i.e., there is a pre-existing momentum component in the plane of collision), the jet will predominantly spread out in the direction of this momentum

component (see Figure 1A). As the sheet spreads out, its thickness, t , is inversely proportional to the distance from the point of the collision as the amount of liquid in the sheet is conserved. Surface tension acts to oppose the spreading, providing the force which draws the sheet back to a point, resulting in the formation of an acute leaf shape and limiting how thin the sheet can be. Hence, the ultimate thickness of the sheet depends on the volume of liquid flowing through the collision point. In order to make the sheet as thin as possible, it needs to be produced with a small volume of liquid, which necessitates the nozzle dimensions being very small, of the order of tens of μm .

Flatjet sheets employed in X-ray spectroscopy and other measurements must also be highly stable. Here, stability is defined by the sheet holding constant thickness and shape for the duration of a measurement, being resistant to break-up and phase changes, as well as maintaining a flat, ripple-free surface with respect to the wavelength and beam size. The primary breakup mechanism that we have observed for these jets arises due to asymmetric surface waves. If these surface waves become large enough relative to the sheet thickness it will cause the sheet to break up into droplets (Huang, 1970; Eggers and Villermaux, 2008), but also they can fluctuate the absorption path length leading to increased noise in absorption measurements. A measure of the relationship between the inertia of the liquid and the viscosity of the liquid is given by the Reynolds number:

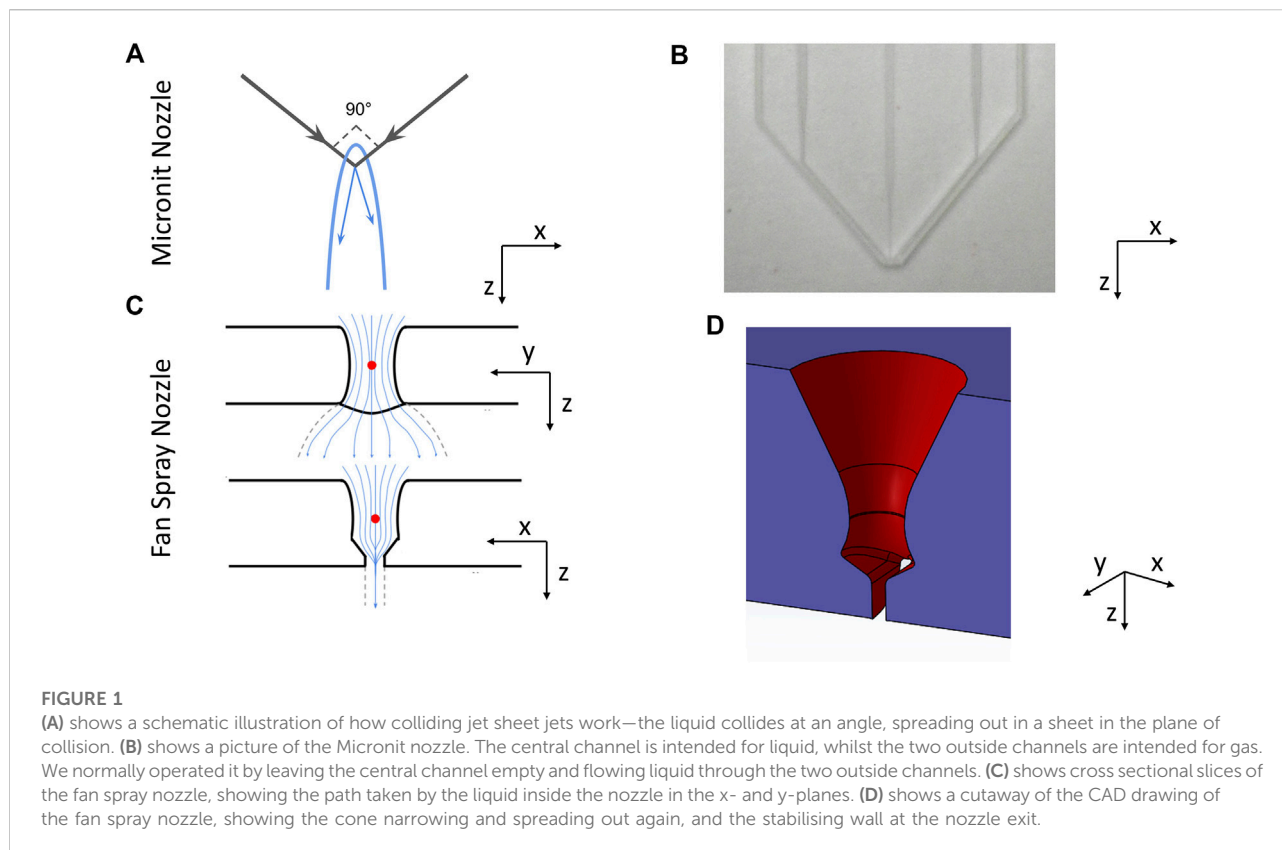
$$\text{Re} = \frac{\rho u L}{\mu}, \quad (1)$$

where ρ is the density of the liquid, u is the velocity of the liquid, L is a characteristic length defined by the parameters of the system under study and μ is the dynamic viscosity of the liquid. Although there are a number of factors that could influence the exact location of the threshold, an estimated figure for the point at which surface waves will cause breakup is given by Huang (1970) as a Reynolds number of approximately 2,000, which is close to the value obtained from our results presented later on in this paper.

2.1 Methods to generate flat sheet jets

The nozzle designs both operate according to the same principles outlined above. However they differ in their details, most notably in their collision mechanisms. The Micronit chip nozzles consist of two plates of borosilicate glass with 50 μm wide channels etched into them. Two channels are set at 90° to each other, whilst the third channel is positioned in between these at 45° to both channels, Figure 1B. This design was first presented by Koralek et al. (2018), and nozzles are commercially available from Micronit GmbH.

The original intended working mode of this nozzle is to flow liquid down the central channel and gas down the side channels.



The momentum of the gas imparts the radial momentum to the liquid, causing it to spread out into the thin flatjet. However in practice the high gas pressures required add complexity and the sheets produced are very small. Thus, we have run this nozzle by flowing liquid through the gas channels which is closer to a “true” collision regime. The momentum that creates the sheet is provided by the streams of liquid themselves, and this method works reliably to produce sheets of desired thickness and stability. In a subsequent paper the authors have improved on this design (Crissman et al., 2022), however at this time the improved design is not available commercially.

The second nozzle was created in-house, as presented in Galinis et al. (2017). This nozzle works by funnelling liquid down into a compression point *via* a cone with an angle 60° to the normal. As shown in Figure 1C, the liquid spreads out uninterrupted along the *y*-axis from this point, allowing the liquid to create a sheet. In the *x*-axis however, the liquid starts to spread out before cutting sharply back in, cancelling out the transverse momentum and ensuring that the sheet spreads out as thin as possible. This design is similar to nozzles used to spray droplets for fuel injection or pesticide spreading (Dombrowski et al., 1960), so it is referred to as a “fan spray” nozzle. A cutaway of this nozzle design is shown in Figure 1D. This specific nozzle is not available commercially, but similar can be manufactured using a commercially

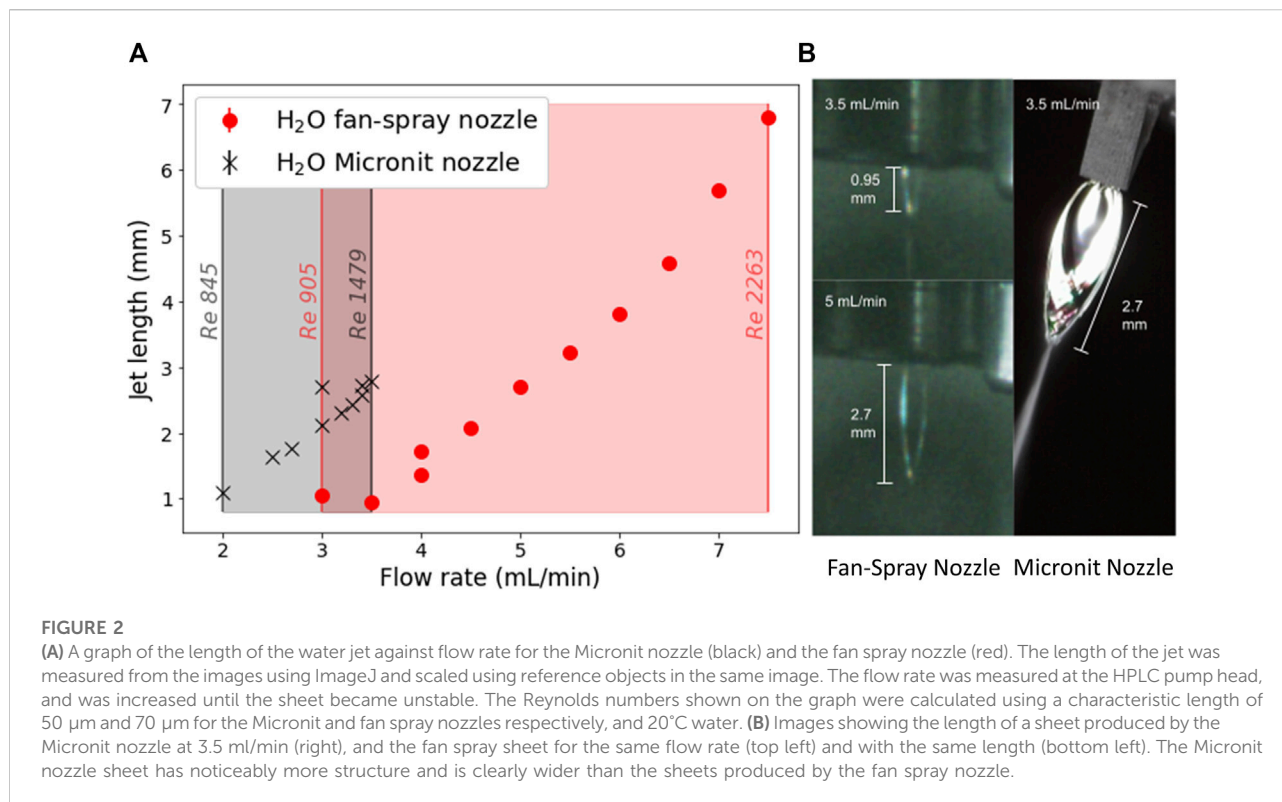
available 3D printer (Photonic Professional GT2, by Nanoscribe GmbH, or *via* ProForNano).

3 Results

3.1 Characteristics of the sheets produced by the microfluidic apparatus

Due to the differences in geometry, the sheets produced by the two nozzles have somewhat different properties. Figure 2 shows a comparison of the length of the sheets produced using water by these two nozzles. The most obvious difference is in the size of the sheets produced—the sheets produced by the Micronit nozzle are significantly longer than those produced by the fan spray nozzle for flow rates below 3.5 ml/min. Beyond this flow rate the sheet produced by the Micronit nozzle becomes unstable. This occurs at 7.5 ml/min for the sheet produced by the fan spray nozzle. Surface waves are noticeably more prominent on the sheets produced by the Micronit nozzle than on those produced by the fan spray nozzle, which is the probable source of instability.

These differences in jet structure can be ascribed to the differences in the geometry around the collision point in the two nozzles. Although the Micronit nozzle does guide the sheet



after collision in some sense, since the liquid is prevented from spreading out in all directions freely due to the presence of the chip itself, it is not designed to actively shape the sheet. Thus, the liquid spreads out approximately as a sheet produced by the standard colliding jets geometry (Taylor, 1959a; Taylor, 1959b; Taylor, 1959c; Taylor, 1960). The fan spray nozzle, however, does purposefully guide the sheet into a desired shape. As shown in Figure 1, after the collision point, the nozzle opens up again at the same angle. It then cuts back to form the slit in one of planes which is effectively a 50 μm long wall on either side of the sheet. This has the effect of determining the maximum thickness of the sheet as it starts to spread out, and also damps any surface waves that may form due to the momentum transfer inside the nozzle.

The greater length of the sheets from the Micronit nozzle at a constant flow rate can be explained as a function of the smaller diameter of the channels that liquid flows through in the chip. They are slightly elliptical, with a major axis of 50 μm and a minor axis of 45 μm , whilst the fan spray nozzle has a minimum diameter of 70 μm . This smaller diameter means that in order to maintain the same flow rate, the liquid needs to flow at a greater velocity. Therefore, at the point of collision there is a greater amount of transverse momentum to be distributed, leading to a larger sheet, and therefore a thinner sheet. As noted in Figure 2, a Reynolds number of around 1,500 the Micronit nozzle sheet becomes unstable, whereas the fan spray sheet is stable up to around 2,300. This extended stability into higher

Reynolds numbers can be attributed to the damping effect of the walls in the nozzle damping out the surface waves.

To compare the sheet thickness we performed interferometry measurements (Galiniš et al., 2017) for sheets produced in isopropanol, with the results shown in Figure 3. The sheet produced by the fan spray nozzle has a shallower gradient along its length than that produced by the Micronit nozzle. The guidance provided in the fan spray nozzle restricts the direction that the liquid can flow, and so we can assume that a greater proportion of the liquid just after the nozzle exit is in the sheet rather than the rims compared to the Micronit nozzle. The liquid then migrates to the rims more gradually, leading to this shallower decay curve.

3.2 Operation of microfluidic jets in vacuum

In order to produce a sheet from these nozzles, pressurised liquid needs to be forced through them. This can be achieved using compressed gas, or using an HPLC (High Pressure Liquid Chromatography) pump (Knauer Azura 6.1 L). We preferred the HPLC pump as it allows for greater control over the flow rates and access to higher backing pressures. The pulsation due to the HPLC pump is damped using a corrugated pipe and an analog pressure meter (Ventura

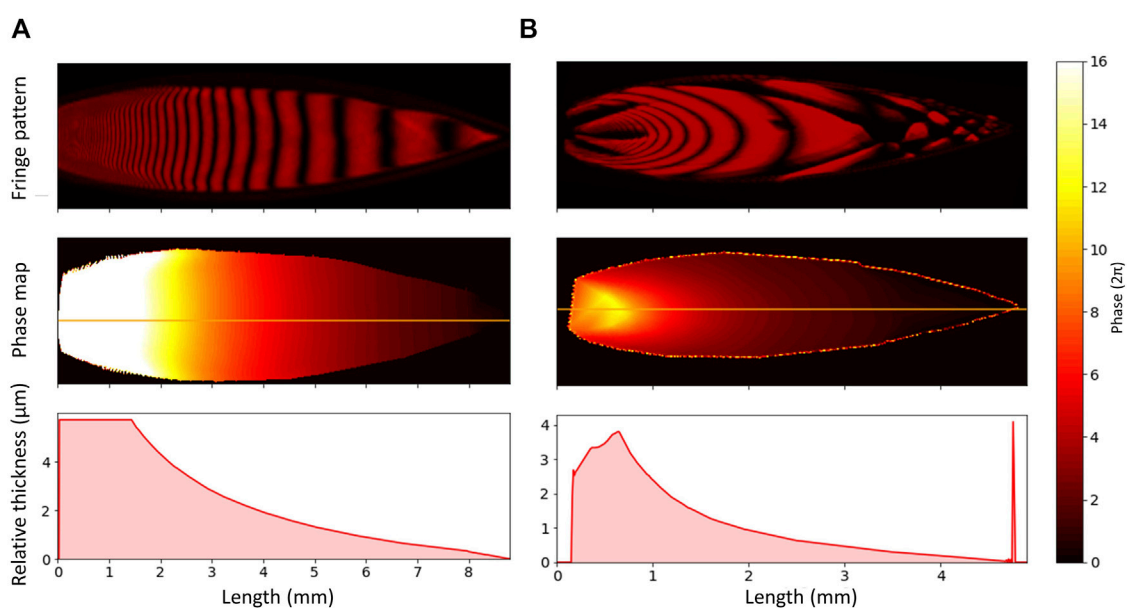


FIGURE 3

Monochromatic interferograms produced by illuminating isopropanol with a 633 nm HeNe laser. **(A)** uses the fan spray nozzle, and **(B)** uses the Micronit nozzle. Below the fringe patterns are some phase maps, produced from the fringe patterns using Jakub Dranczewski's Magic2 package (Dranczewski, 2021). The bottom panel shows the change in relative thickness along the centerline of the sheet, indicated on the phase map. The phase near the nozzle becomes unreliable due to the fact that the lines become so close together that the camera cannot resolve them properly. In reality, the thickness should continue to increase smoothly. The spike in the thickness profile in column **(B)** is an artefact due to light scatter from the rim of the sheet.

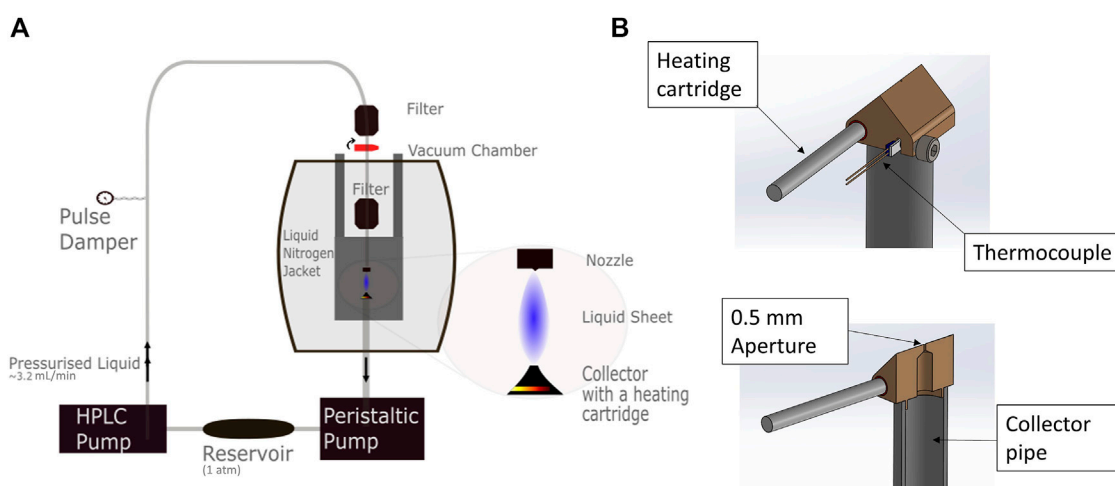
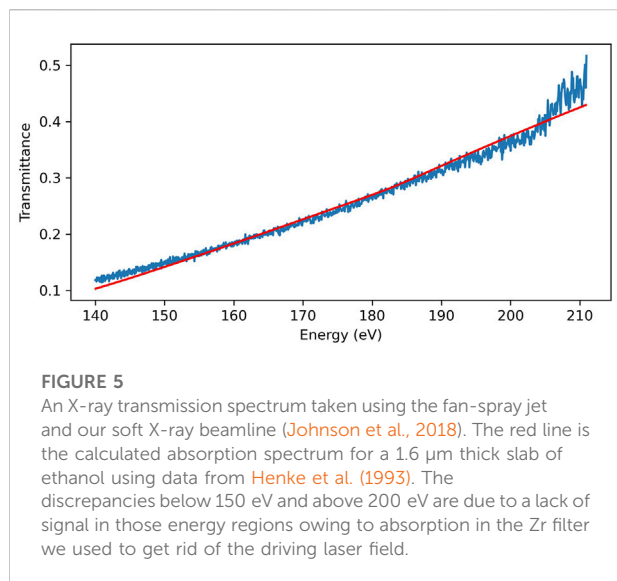


FIGURE 4

(A) A sketch of our recirculating system. The liquid is pumped from an atmospheric pressure reservoir by the HPLC pump into the nozzle, where it creates the sheet. The collector tip is heated to 60° by a 25 W heating cartridge. A thermocouple is attached to the collector tip to ensure a constant temperature is maintained. The liquid is then pumped from vacuum to atmosphere by a peristaltic pump (Gilson Minipuls 3). The analogue pulse damper is attached to the high pressure side, and eliminates the pulsation due to the HPLC pump. **(B)** Schematics of our catcher head, showing the heating cartridge and thermocouple attachments for temperature stabilisation, and the small aperture to reduce backflow.



and Nikelly, 1978) inserted between the pump output and chamber input. Blocking of the nozzles is minimised by two 2 μm pore inline filters in the high pressure line before the nozzle.

Our recirculating system is shown in Figure 4. The liquid is pumped from the atmospheric pressure of the reservoir through the nozzle, where it produces a sheet. This sheet is then fed into the catcher, taking care that the tip of the leaf is located in the aperture to minimise splashing. The catcher is a triangular prism made of phosphor bronze (for greater thermal conductivity). The aperture is small (0.5 mm diameter) to prevent gas backflow from the pipe below the catcher, and the catcher also has a resistive heating tube and a thermocouple installed in order to control its temperature. The liquid caught by the catcher is then pumped back to the atmospheric pressure reservoir by a peristaltic pump (Gilson Minipuls 3), which allows for recirculation.

However, recirculation of volatile liquids, which includes many common solvents, still provides a significant challenge. Due to the geometry of our chamber the distance between the collector and the peristaltic pump is around a meter, which is a great enough distance for a high vapour pressure liquid to evaporate before it is pumped into the reservoir. Recirculating these liquids requires attention to the rate of evaporation, making the distance from the collector to the peristaltic pump as short as possible and optionally cooling the collector to further reduce the volatility.

The vacuum in the chamber is maintained by a liquid nitrogen jacket, which surrounds the liquid jet apparatus and traps most of the vapour. In this way we are able to maintain the ambient pressure in the chamber at 1×10^{-3} mbar or below.

3.3 X-ray absorption in ethanol

The purpose of these flatjets is to perform soft X-ray spectroscopy on them, and an X-ray transmission spectrum of ethanol is shown in Figure 5. The ethanol sheet was created using the fan-spray nozzle and this spectrum was taken using soft X-rays produced by HHG in neon. The jet was aligned such that the X-rays passed through the center of the sheet, and the measured transmission coefficients agree well with calculated ones based on data from (Henke et al., 1993) for a 1.6 μm thick sheet. This value accords well with the thickness values measured by interferometry in (Galiniš et al., 2017), and as such provides us with an independent verification of the thickness of our jet in vacuum under these conditions.

4 Discussion

4.1 Temperature and evaporation of the jet as it propagates in vacuum

As the jet expands into vacuum molecules will evaporate from the surface, cooling the liquid. To perform XUV spectroscopy it is essential that a vacuum is maintained, but also that there is knowledge of the temperature of the liquid as this may impact reaction rates and absorption features in large organic molecules. To this end we can calculate the cooling and evaporation from the sheet. The number of molecules evaporating from an area A is assumed to follow the Hertz-Knudsen equation:

$$\frac{dN}{dt} = \frac{A(p_{\text{vap}} - p)}{\sqrt{2\pi mk_b T}}, \quad (2)$$

where p_{vap} is the vapour pressure of the liquid, p is the partial pressure of the vapour surrounding the liquid and T is the temperature of the liquid. Following the treatment in Heissler et al. (2014) [based on Faubel et al. (1988)], the change in jet temperature due to this evaporation is

$$dT = -\alpha \frac{H_{\text{vap}}}{C_p}, \quad (3)$$

where H_{vap} is the enthalpy of vapourisation, α is the ratio of evaporated molecules to molecules remaining in the jet and C_p is the specific heat capacity of the liquid. Due to relatively high liquid flow rates in our jets, we assume the change in mass due to evaporation is negligible so we write α as:

$$\alpha = \frac{dN}{N_A M}, \quad (4)$$

where M is the mass of the liquid in the jet. The change in temperature over time as the jet expands into the vacuum is therefore:

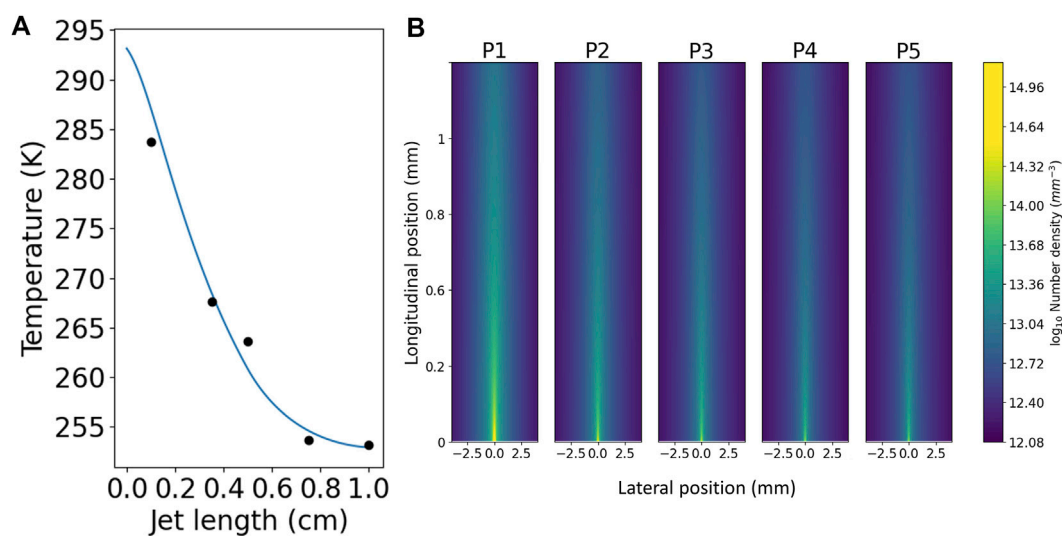


FIGURE 6

The relationship between jet length, temperature and pressure. **(A)** The blue curve shows the expected temperature decrease over its length for a 1 cm long diamond shaped jet of isopropanol that is 1 mm wide at its middle with a flow rate of 9.1 ml/min. The black dots are experimental data taken under similar conditions, measured by manually inserting a thermocouple into the sheet. **(B)** The horizontal vapour distribution at the same vertical positions as the experimental data (listed as P1-5, with one being closest to the nozzle). As can be seen, by the bottom of the sheet (the thinnest and flattest part, ideal for taking measurements), the vapour density has dropped by two orders of magnitude.

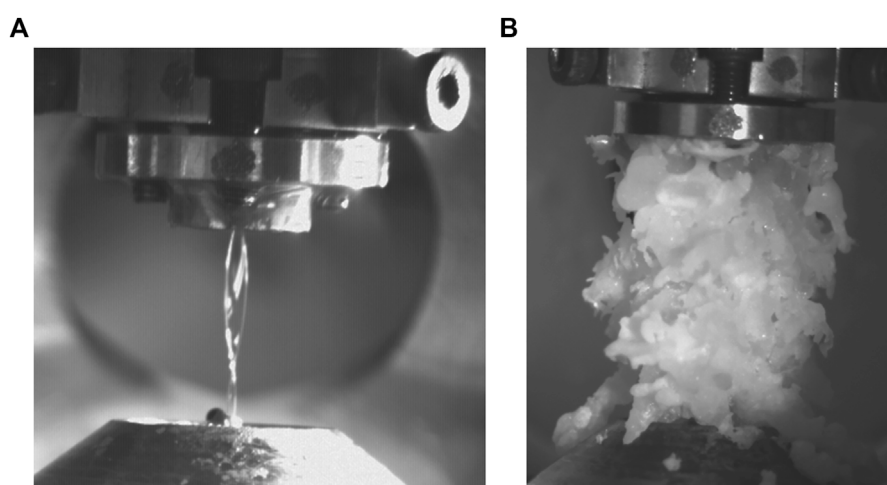


FIGURE 7

(A) before and **(B)** after images of catastrophic freezing in a jet of DMSO. The ice grows to this size in less than a second.

$$\frac{dT}{dt} = \frac{H_{\text{vap}} A (p_{\text{vap}} - p)}{-C_p N_A M \sqrt{2\pi m k_b T}} \quad (5)$$

$$\rho_{\text{vap}} = \frac{\rho_0}{x^2 + y^2 + z^2}. \quad (6)$$

In order to model the distribution of vapour around the jet we start with the vapour density at position (x, y, z) due to a point source at the origin

We can then expand the point source into a rectangular surface of width w and height h , and find the vapour distribution at a distance r from the surface

$$\rho_{\text{vap}}(x, y, r) = \int_{-\frac{w}{2}-y}^{\frac{w}{2}-y} \int_{-\frac{h}{2}-x}^{\frac{h}{2}-x} \frac{\rho_0(x, y)}{x^2 + y^2 + r^2} \quad (7)$$

Using these equations we calculate the temperature and consequent vapour pressure of the jet, as well as the distribution of the vapour, as can be seen in Figure 6. Recent work by the Wolf group (Chang et al., 2022) showed much more rapid evaporation and cooling in an alcohol than we have measured. This is probably due to the shape of the jet—theirs likely becomes much wider much more quickly, leading to a greater initial surface area and consequently faster evaporation and cooling.

4.2 Mitigation of freezing due to adiabatic expansion

As the jet propagates in the vacuum it cools dramatically, cooling 40 K over a 1 cm distance (see Figure 6). If the temperature of the jet drops below the melting point then the liquid is at risk of freezing. If the critical point is at a pressure higher than the ambient pressure in the vacuum chamber, the material does not exist in the liquid phase at equilibrium. For example, we find water and dimethyl sulfoxide (DMSO) to be highly susceptible to freezing. Figure 7 shows unwanted freezing of DMSO which began at the catcher and quickly grew to cover the whole system. This not only halts the experiments but it can damage fragile nozzles, directly leading to failure in many cases.

In order to avoid the issue of freezing the collector tip can be heated—this is area where ice crystals are most likely to nucleate (see Figure 4B for details). Freezing can also be prevented by slowly decreasing the pressure in the chamber when going to vacuum. This avoids a rapid cooling of the sheet and vapour due to adiabatic expansion and has the advantage that alignment from nozzle to catcher is better preserved. This ensures the expansion process is as isothermal as possible, so the liquid is always evaporating rather than freezing, and avoids spillages of liquid into the chamber. It is important to do this with the jet running, as stationary water will freeze in the nozzle under vacuum.

5 Conclusion

Thin liquid sheet jets constitute a development of high utility for performing soft X-ray experiments in vacuum. Thin sheets allow the X-rays transmit with minimal reabsorption, and the opening of X-ray spectroscopy experiments to the liquid and solution phases allows a wider range of chemical and biological systems to be studied in their natural environment.

We have compared two types of thin liquid sheet jet, both of which make sheets thin enough for soft X-ray experiments. The fan spray nozzle will make sheets that are slightly thicker than the Micronit nozzle, but the sheets are also more stable with less structure due to surface waves. Both can be run in vacuum using the same apparatus,

and if used with care can prove useful as targets for soft X-ray experiments in liquids. Nozzles represent a far lower setup cost than two colliding cylindrical microjets, the other widespread method of creating 1 μm thick sheets of liquid in vacuum, owing to the fact that they do not need to be aligned. The nozzle presented by Koralek et al. (2018) is commercially available, and therefore a good general solution, however for those with the resources to make the nozzle presented in Galinis et al. (2017), we recommend it as an alternative solution if larger target areas are desired.

Data availability statement

The raw data supporting the conclusion of this article will be made available by the authors, without undue reservation.

Author contributions

JB: Equipment design, data collection and analysis, figure creation, principal author JL: Data collection, manuscript drafting OA: Data collection, manuscript drafting SJ: Data collection, equipment design DG: Data collection RP: Data collection, manuscript drafting KK: Data analysis, figure creation, manuscript drafting CF: Data collection, figure creation, manuscript drafting AG: Equipment design and manufacture MM: Manuscript drafting and critical revision JM: Manuscript drafting and critical revision.

Funding

Defence Science and Technology Laboratory (MURI EP/N018680/1), lab funding; Engineering and Physical Sciences Research Council (EP/N018680/1, EP/T006943/1, EP/R511547, EP/I032517/1), lab funding and impact acceleration grant; Marie Curie (641272), PhD funding for SJ.

Acknowledgments

We gratefully acknowledge Gediminas Galinis for the original design and manufacture of the fan-spray nozzle, Susan Parker and Conor O'Donovan for technical help in performing the experiments, and Omri Tau, Will Fortune and Joey Broughton for useful discussions on the subject of liquid jets.

Conflict of interest

The authors declare that the research was conducted in the absence of any commercial or financial relationships that could be construed as a potential conflict of interest.

Publisher's note

All claims expressed in this article are solely those of the authors and do not necessarily represent those of their affiliated

organizations, or those of the publisher, the editors and the reviewers. Any product that may be evaluated in this article, or claim that may be made by its manufacturer, is not guaranteed or endorsed by the publisher.

References

- Attar, A. R., Bhattacharjee, A., and Leone, S. R. (2015). Direct observation of the transition-state region in the photodissociation of CH₃I by femtosecond extreme ultraviolet transient absorption spectroscopy. *J. Phys. Chem. Lett.* 6 (24), 5072–5077. doi:10.1021/acs.jpcclett.5b02489
- Chang, Y. P., Yin, Z., Balcianas, T., Jakob Wörner, H., and Wolf, J. P. (2022). Temperature measurements of liquid flat jets in vacuum. *Struct. Dyn.* 9 (1), 014901. doi:10.1063/4.0000139
- Crisman, C. J., Mo, M., Chen, Z., Yang, J., Huyke, D. A., Glenzer, S. H., et al. (2022). Sub-micron thick liquid sheets produced by isotropically etched glass nozzles. *Lab. Chip* 22 (7), 1365–1373. doi:10.1039/d1lc00757b
- Dombrowski, N., Hasson, D., and Ward, D. E. (1960). Some aspects of liquid flow through fan spray nozzles. *Chem. Eng. Sci.* 12 (1), 35–50. doi:10.1016/0009-2509(60)87012-1
- Dranczewski, J. (2021). Magic2. Available at: <https://github.com/jdranczewski/Magic2>.
- Eggers, J., and Villermaux, E. (2008). Physics of liquid jets. *Rep. Prog. Phys.* 71 (3), 036601. doi:10.1088/0034-4885/71/3/036601
- Ekimova, M., Wilson, Q., Faubel, M., Wernet, P., and Nibbering, T. J. (2015). A liquid flatjet system for solution phase soft-x-ray spectroscopy. *Struct. Dyn.* 2 (5), 054301. doi:10.1063/1.4928715
- Faubel, M., Schlemmer, S., and Toennies, J. P. (1988). A molecular beam study of the evaporation of water from a liquid jet. *Z. Phys. D - Atoms Mol. Clust.* 10 (2-3), 269–277. doi:10.1007/bf01384861
- Galinis, G., Strucka, J., Jonathan, C., Barnard, T., Braun, A., Smith, R. A., et al. (2017). Micrometer-thickness liquid sheet jets flowing in vacuum. *Rev. Sci. Instrum.* 88 (8), 083117. doi:10.1063/1.4990130
- Garratt, D., Misiak, L., Wood, D., Larsen, E. W., Matthews, M., Alexander, O., et al. (2022). Direct observation of ultrafast exciton localization in an organic semiconductor with soft X-ray transient absorption spectroscopy. *Nat. Commun.* 13 (1), 3414. doi:10.1038/s41467-022-31008-w
- Goulielmakis, E., Schultze, M., Hofstetter, M., Yakovlev, V. S., Gagnon, J., Uiberacker, M., et al. (2008). Single-cycle nonlinear optics. *Science* 320 (5883), 1614–1617. doi:10.1126/science.1157846
- Henke, B. L., Gullikson, E. M., and Davis, J. C. (1993). X-ray interactions: Photoabsorption, scattering, transmission, and reflection at E = 50–30, 000 eV, Z = 1–92. *At. Data Nucl. Data Tables* 54 (2), 181–342. doi:10.1006/adnd.1993.1013
- Ha, B., Deponte, D. P., and Santiago, J. G. (2018). Device design and flow scaling for liquid sheet jets. *Phys. Rev. Fluids* 3 (11), 114202. doi:10.1103/physrevfluids.3.114202
- Heissler, P., Lugovoy, E., Horlein, R., Waldecker, L., Wenz, J., Heigoldt, M., et al. (2014). Using the third state of matter: High harmonic generation from liquid targets. *New J. Phys.* 16, 113045. doi:10.1088/1367-2630/16/11/113045
- Huang, J. C. P. (1970). The break-up of axisymmetric liquid sheets. *J. Fluid Mech.* 43 (2), 305–319. doi:10.1017/s0022112070002392
- Johnson, A. S., Wood, D., Austin, D. R., Brahms, C., Gregory, A., Holzner, K. B., et al. (2018). Apparatus for soft x-ray table-top high harmonic generation. *Rev. Sci. Instrum.* 89 (8), 083110. doi:10.1063/1.5041498
- Jordan, I., Huppert, M., Rattenbacher, D., Peper, M., Jelovina, D., Perry, C., et al. (2020). Attosecond spectroscopy of liquid water. *Sci. (80-.)* 369 (8), 974–979. doi:10.1126/science.abb0979
- Joseph, D., Li, S., Driver, T., Champenois, E. G., MacArthur, J. P., Lutman, A. A., et al. (2020). Tunable isolated attosecond X-ray pulses with gigawatt peak power from a free-electron laser. *Nat. Photonics* 14 (1), 30–36. doi:10.1038/s41566-019-0549-5
- Koralek, J. D., Kim, J. B., Brůža, P., Curry, C. B., Chen, Z., Bechtel, H. A., et al. (2018). Author Correction: Generation and characterization of ultrathin free-flowing liquid sheets. *Nat. Commun.* 9 (1), 1615. doi:10.1038/s41467-019-09457-7
- Schnorr, K., Bhattacharjee, A., Oosterbaan, K. J., Delcey, M. G., Yang, Z., Tian, X., et al. (2019). Tracing the 267 nm-induced radical formation in dimethyl disulfide using time-resolved X-ray absorption spectroscopy. *J. Phys. Chem. Lett.* 10 (6), 1382–1387. doi:10.1021/acs.jpcclett.9b00159
- Smith, A. D., Chang, Y. P., Schmidt, C., Zinchenko, K., Nunes, F. B., Rossi, E., et al. (1988). Femtosecond soft-X-ray absorption spectroscopy of liquids with a water-window high-harmonic source. *J. Phys. Chem. Lett.* 11 (6), 1981–1988. doi:10.1021/acs.jpcclett.9b03559
- Taylor, G. (1959). Dynamics of thin sheets of fluid III. Disintegration of fluid sheets. *Proc. R. Soc. A Math. Phys. Eng. Sci.* 253, 313–321.
- Taylor, G. (1960). Formation of thin flat sheets of water. *Proc. R. Soc. A Math. Phys. Eng. Sci.* 259.
- Taylor, G. (1959). The dynamics of thin sheets of fluid II. Waves on fluid sheets. *Proc. R. Soc. A Math. Phys. Eng. Sci.* 253, 296–312.
- Taylor, G. (1959). The dynamics of thin sheets of fluid. I. *Proc. R. Soc. A Math. Phys. Eng. Sci.* 253 (1274), 289–295.
- Ventura, D. A., and Nikelly, J. G. (1978). Pulse dampening system for high pressure liquid Chromatography. *Anal. Chem.* 50 (7), 1017–1018. doi:10.1021/ac50029a052